A HIGH-SPEED MULTI-CHEMISTRY AND MULTI-BATTERY STATE-OF-HEALTH SCREENING SYSTEM FOR RETIRED LITHIUM-ION BATTERIES

Teodor-Iulian VOICILA[1], Bogdan-Adrian ENACHE[2], Mihaela-Viorica MATEESCU[3], George-Calin SERITAN[4]

The transition to sustainable energy solutions is driving the automotive sector to shift from internal combustion engine vehicles to electric and hybrid vehicles, aligning with global objectives of reducing greenhouse gas emissions and achieving carbon neutrality. However, the exponential growth of the latter's adoption introduces challenges in managing end-of-life lithium-ion batteries, which are expected to reach unprecedented volumes in the coming decades. Although no longer suitable for automotive applications, these batteries often retain about 80% of their initial capacity, making them viable for "second-life" applications, extending their lifecycle, reducing costs, and supporting the circular economy. Proper evaluation and classification of these batteries are essential to ensure safety and effective repurposing to less demanding applications. This study introduces an intelligent system and a new methodology for fast, cost-effective, and adaptable screening of retired lithium-ion batteries. The system's modular design, centered on a cascaded Buck-Boost DC-DC converter, enables simultaneous testing of multiple batteries, halving testing time. Also, the wide input/output voltage range allows diverse battery chemistries and configurations to be tested. Integrating a presorting stage based on internal resistance measurements minimizes the need for exhaustive state-of-health evaluations of individual batteries. Validation experiments conducted on ten LFP battery cells across varying ageing levels (86%–95%) demonstrated the effectiveness of the proposed approach, achieving accurate grouping within a 2% error margin. Then, the representative battery from each group can be evaluated using a standard long-duration, highly accurate method.

Keywords: Battery screening system, LiFePO4, Retired batteries, State-of-Health

[1] PhD Student, Department of Measurement, Electrical Devices and Static Converters, National University of Science and Technology POLITEHNICA Bucharest, Romania, e-mail: iulian.voicila@upb.ro

[2] Associate Professor, Department of Measurement, Electrical Devices and Static Converters, National University of Science and Technology POLITEHNICA Bucharest, Romania, e-mail: bogdan.enache2207@upb.ro

[3] Lecturer, Department of Measurement, Electrical Devices and Static Converters, National University of Science and Technology POLITEHNICA Bucharest, Romania, e-mail: mihaela.mateescu@upb.ro

[4] Professor, Department of Measurement, Electrical Devices and Static Converters, National University of Science and Technology POLITEHNICA Bucharest, Romania, e-mail: george.seritan@upb.ro

1. Introduction

The world is trying to reduce greenhouse gas emissions and combat climate change, which has made carbon neutrality a key global objective [1]. Thus, the increasing demand for sustainable energy solutions is reshaping industries worldwide, especially the automotive sector, which is undergoing a transition from internal combustion engine (ICE) vehicles to electric vehicles (EVs) and hybrid electric vehicles (HEVs) [2]. However, the rapid growth end-of-life (EOL) of lithium-ion batteries led to an unprecedented volume of batteries reaching their EOL within the next few decades [3]. Traditionally, EOL batteries involve recycling, which, while effective in recovering valuable materials, is an expensive and environmentally taxing process that generates significant waste and pollution [4]. Recycling also fails to fully leverage the remaining energy potential of these batteries, which often still retain about 80% of their initial capacity [5]. This untapped potential has driven interest in "second-life" applications, where batteries are repurposed for less demanding uses, such as energy storage for renewable sources, backup power systems, and low-power consumer devices [6]. By extending the life cycle of batteries, this concept can significantly reduce costs, decrease environmental impact, and support the circular economy [7].

An effective sorting and evaluation process is essential to facilitate the integration of retired batteries. This process must accurately assess each battery's state of health (SOH) to ensure its suitability for repurposing. Generally, the screening process has two phases. First, the batteries are visually inspected for any visible physical damage. The visual inspection initiates the process by eliminating batteries with potential defects such as corrosion, swelling, and material leakage [8]. Therefore, only batteries that pass the first test can be evaluated in the second phase, where they will be subjected to sorting methods. This stage assesses the SOH and classifies the batteries according to certain criteria that depend on the battery chemistry and the energy application’s requirements [9]. Traditional battery sorting methods, such as complete charge-discharge cycles, Coulomb counting or Electrochemical Impedance Spectroscopy, are often slow, costly, and tailored to specific battery models, limiting their scalability and adaptability [10]. The fastest and easiest to implement methods are DC ohmic resistance and AC ohmic resistance, but they are often sensitive to external factors and have low accuracy [11], [12]. Hybrid methods incorporating intelligent algorithms (e.g., neural networks, fuzzy logic) and conventional methods offer improved accuracy but require substantial computational resources and complex training data, which can hinder their practical application [13], [14]. Analyzing the methods mentioned reveals that they fall into one of two categories: either fast methods with relatively low precision and low/medium complexity or slow and complex but have very high accuracy.

An essential first step in the widespread reuse of EOL batteries is accurate SOH estimation, which enables quick and precise classification. Given that numerous battery pack models may be collected and processed at centralized recycling facilities, the underlying electrochemistry of the various packs, modules, and cells often differs. Individual modules or cells within the same pack may exhibit varying SOH levels due to differences in cycling conditions, temperatures, charge and discharge rates [15]. These factors contribute to significant variation in SOH levels, making the screening process a crucial prerequisite for regrouping batteries effectively. To ensure efficiency, a reliable system for SOH battery evaluation must balance speed and accuracy, employing a combination of methods to address these challenges. SOH assessment must also consider safety concerns, which implies that the evaluation should address each cell due to inconsistent packs/modules [16]. While future battery management systems (BMSs) are expected to incorporate advanced SOH determination capabilities to support second-life applications, the broader retirement process-encompassing transportation, storage, module dismantling, fabrication of new modules, and actual testing, remains time-intensive [17], [18], [19]. This prolonged process introduces further complications; as batteries undergo these administrative and logistical steps, their SOH may degrade due to the lack of real-time monitoring. Addressing these challenges, this research proposes a novel intelligent screening system designed to enhance the evaluation and classification of EOL lithium-ion batteries from the automotive industry. The proposed system integrates an intermediate presorting stage that significantly reduces testing time by grouping batteries based on a fast-screening method. This presorting is followed by a detailed evaluation of a representative battery from each group using established methods, ensuring accurate SOH determination while minimizing overall testing efforts.

The principal contributions of this paper are delineated as follows:

- Proposing a new methodology for screening end-of-life batteries (Section 2);
- Proposing a multi-chemistry, multi-battery screening system (Section 2);
- System validation by analyzing ten aged LFP batteries (Section 3).

2. Materials and methods

The intelligent sorting system proposed in this study aims to address the limitations of conventional battery sorting methods by integrating an innovative approach that reduces testing time, enhances accuracy, and provides scalability.

A. Battery screening methodology

The system combines a presorting stage based on internal resistance with a detailed evaluation of a representative battery from each group, ensuring that battery classification is efficient and reliable, Fig. 1.

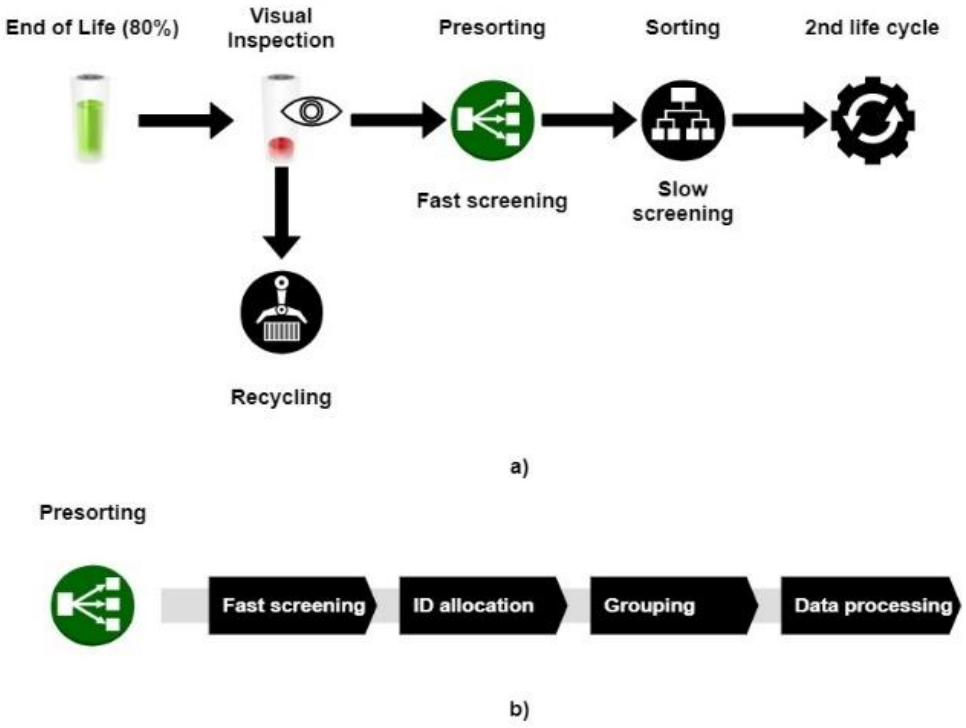

Fig. 1. Proposed methodology for screening retired batteries – a) integration of the presorting phase b) detailed presorting process.

The presorting stage is a crucial step in the proposed methodology, designed to minimize the overall testing time by eliminating batteries that do not meet the basic criteria for reuse. This stage involves a quick assessment of the internal resistance of each battery, which serves as an indicator of the battery's health and consistency with other batteries in the group, as studied in [20]. The presorting process includes the following key steps:

1. **Fast screening**: Initially, a novel regression model based on knee/elbow point is used for precise open circuit voltage (OCV) estimation of the batteries and characterizing their state of charge (SOC) according to OCV. Next, each battery is subjected to a controlled DC pulse for 18 seconds, which can be either a charge or discharge pulse depending on the battery’s initial state of charge (SOC), Fig. 2. The duration and amplitude of the pulse are set according to established standards, such

as the US Advanced Battery Consortium (USABC) manual [21], to ensure consistency and reliability of the measurements.

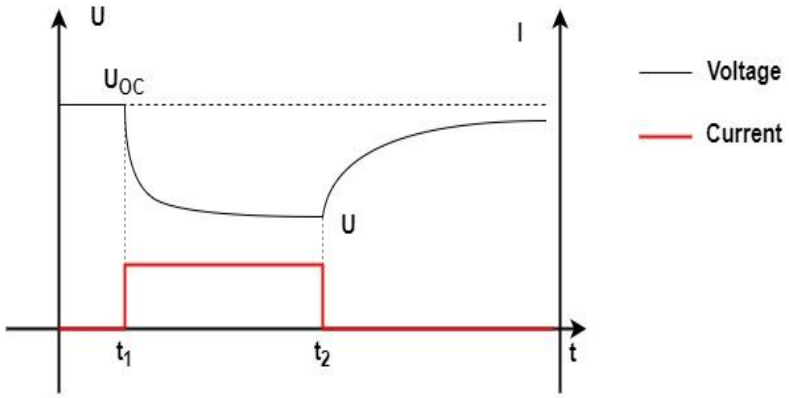

Fig. 2. Proposed methodology for screening retired batteries – a) integration of the presorting phase b) detailed presorting process.

After the pulse ends, the voltage at the battery terminals is measured again, and the internal resistance is determined using Ohm's law, equation 1:

$$R_{in} = \frac{U(t_2) - U(t_1)}{I_{pulse}} \tag{1}$$

where $U(t_1)$ is the OCV, $U(t_2)$ is the voltage after the pulse and I_{pulse} is the applied charge/discharge current.

This simple yet effective approach allows for rapid assessment without the need for complex equipment or prolonged testing procedures.

2. **ID allocation**: At the end of the presorting phase, each battery receives an identifier consisting of three elements: a unique identification number regarding the battery chemistry and the sequence number within the measurement process, the battery's SOC, and the internal resistance.

3. **Grouping**: after the testing is done, battery groups are formed from 10 mΩ to 10 mΩ starting from the battery with the lowest internal resistance.

4. **Data processing**: The mean value and the standard deviation are calculated for each group formed to ensure homogeneity within each group. Batteries that exceed the acceptable range of variation are flagged and either excluded or subjected to additional evaluation.

After all groups have been checked and the outliers eliminated, the sorting phase is applied to a single battery closest to the average value in the group. This battery is selected for detailed testing using a slow but highly accurate method, such as Electrochemical Impedance Spectroscopy (EIS). Based on the SOH results of the representative battery, the entire group is classified for potential second-life applications. Groups with high SOH are designated for more demanding

applications, while those with lower SOH are allocated to less critical uses. This hierarchical sorting ensures that each battery is optimally utilized according to its remaining capacity and performance characteristics. Moreover, this approach drastically reduces the number of batteries requiring complete testing, reducing time, costs, and resource utilization.

B. System implementation

From the hardware point of view, the core of the system is a four-quadrant bidirectional DC-DC power converter, studied in detail in [22]. This power converter enables simultaneous charge and discharge testing of multiple battery cells, allowing for rapid evaluation and classification. Its design optimizes the power transfer between batteries, allowing one battery to act as a power source and the other as a load. The converter's power density and flexibility enhance the system's ability to evaluate a variety of battery chemistries, making it suitable for a wide range of applications beyond the automotive sector. Thus, the modular and scalable nature of the system allows for easy adaptation and expansion, making it capable of handling larger battery packs or different configurations as needed. The electrical diagram of the proposed control and power circuits is presented in Fig. 3. The diagram consists of five functional blocks:

- Power supply block: both the control circuit and the power circuit are powered by a battery with a voltage higher than 14 V. This voltage passes through two step-down converters to power the control circuit at 5 V and the power drivers at 12 V. The use of batteries to power the circuit allows the solution to be used on site.
- Test block: This block contains the bidirectional DC-DC converter and the 2N batteries to be tested. The power circuit has four operating scenarios: voltage step-down from left to right and vice versa, voltage step-up from left to right, and inverse.

Control block: The microcontroller (ESP32) provides the control signals for the power converter based on the battery terminal voltage and OCV. It is also responsible for processing data from current and voltage sensors to determine the internal resistance of the tested batteries.

User interface block: This is achieved using two buttons for inserting test data and initializing the test and a 2x16 LCD display for viewing data.

Protection block: From a hardware point of view, protection is achieved by the diodes, which don't allow energy transfer between the batteries when the circuit is not controlled. By software means, the microcontroller turns off the power switches in case of overvoltage, undervoltage, short circuit, or other operating anomalies.

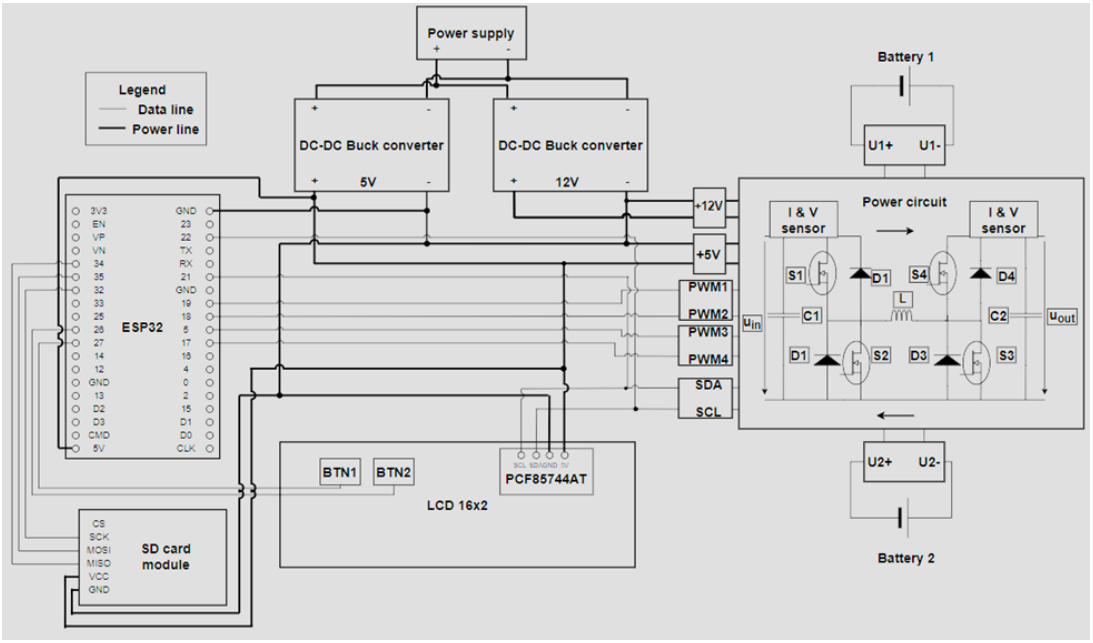

Fig. 3. Electrical diagram of the proposed system (control circuit and power circuit).

Fig. 4 presents the top view of the designed device. The power circuit for battery testing is in the upper area. In the lower area, we have the user interface block (LCD and buttons), the SD card module, the microcontroller, and the power supply block containing a holder for four 18650 batteries.

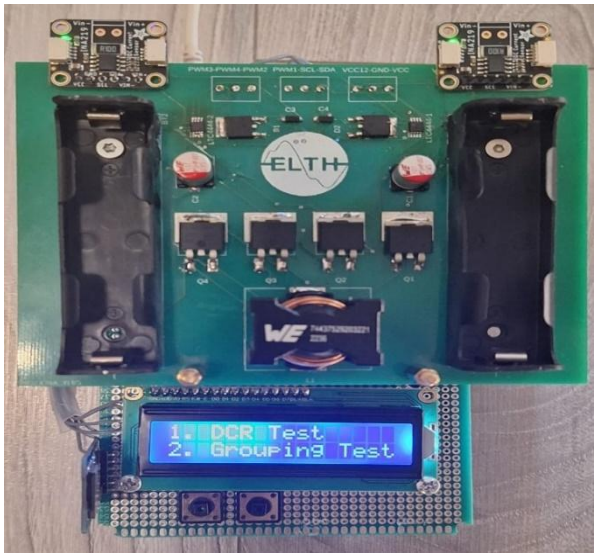

Fig. 4. Prototype of the proposed system (top view).

The control logic implemented within the ESP32 microcontroller is shown in Fig. 5.

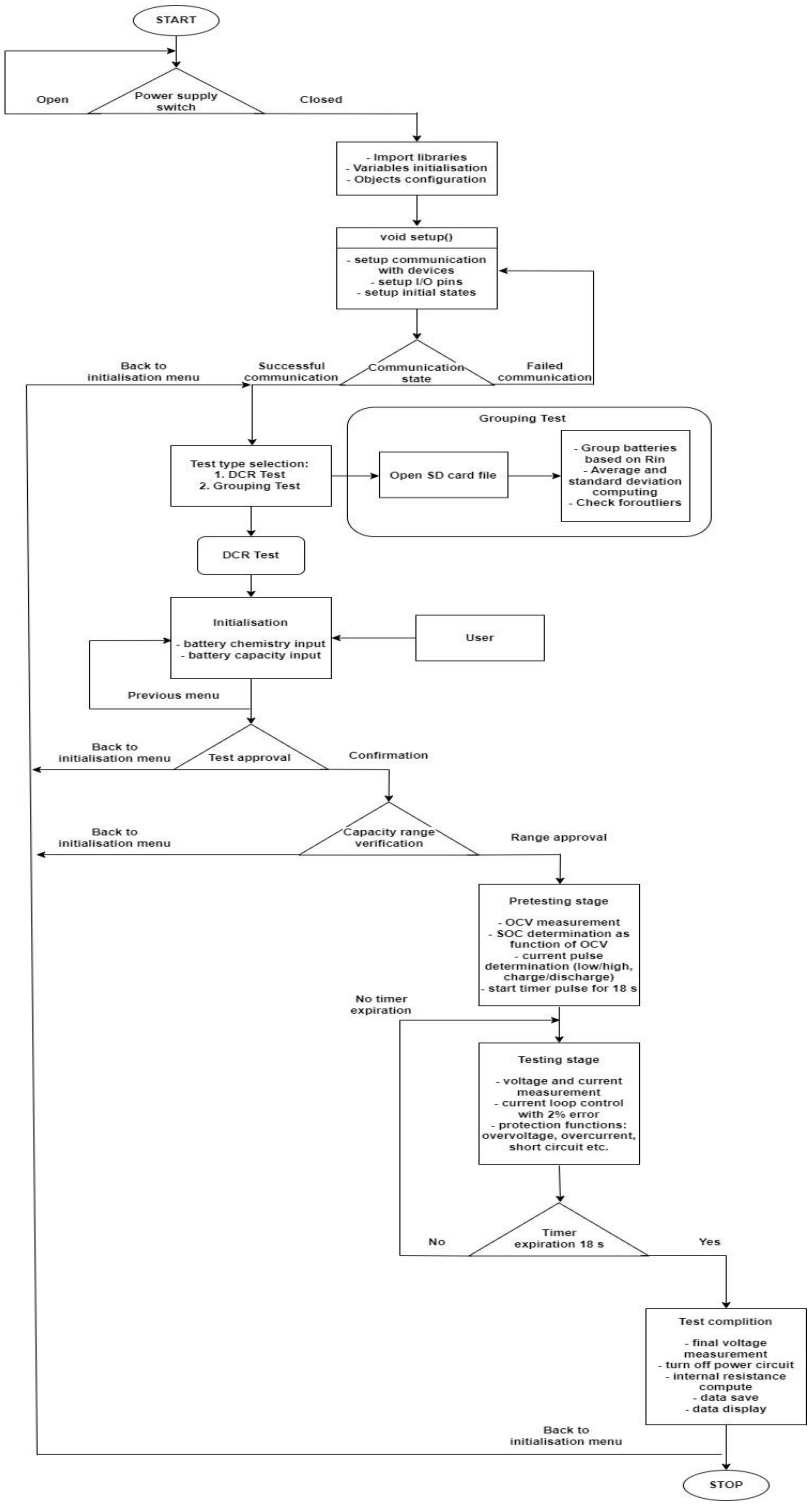

Fig. 5. System software flowchart.

The initialization of the testing process is carried out using a general switch that powers the entire circuit. This also acts as a general protection function. If the switch is closed, then the global variables are read from the ROM memory, and the object configuration is initialized. In the main loop of the code, the input/output pins (PWM, SDA, SCL, DAC, ADC) are configured, as well as their initial state (high, low, digital output, digital input and so on), and communication with the devices is established. The sequence for entering the test parameters cannot be initialized until communication is established. The device will repeat the communication sequence until it is valid. A device reset will be required if the result is invalid after multiple attempts. In the initialization phase of the procedure, the user is expected to choose the type of test, DCR Test or Grouping Test. DCR Test is the sequence through which the internal resistance of the batteries is evaluated and requires the introduction of the following input parameters: the battery chemistry (LFP, NMC, LiPo, etc.) and capacity (900 mAh, 1100 mAh, etc.). After the test is approved, there is a first stage of checking the capacity range, and then the pre-test stage follows. Here, the OCV measurement function is called to determine the SOC of the batteries based on the developed models. Also, the current pulse is calculated as C/4 of the capacity, and it is determined which battery will be charged and which will be discharged, as well as the operating mode of the power converter (forward Buck, reverse Boost, reverse Buck, forward Boost). After this pre-testing stage, a timer is started for 18 seconds, during which the charge/discharge current pulse is applied. The battery voltage and current are monitored for the control loops and provide protection.

After the timer is finished, the power circuit is stopped, and the data processing phase is started. In this last stage, the internal resistance of the batteries is calculated and saved onto an SD card along with the other parameters. The program returns to the initialization menu after each DCR Test. After all the batteries on the site have been tested, the Grouping Test option can be selected. This test will access the file loaded on the SD card and run the battery grouping function mentioned above.

3. Results and discussions

To validate the proposed system, a series of experiments was conducted using ten LFP battery cells grouped into four sub-lots based on their SOH. Each sub-lot represented different ageing levels, ranging from 86% to 95% SOH (Table 1).

Table 1

SOH values of the tested batteries

Battery ID	Nominal capacity [mAh]	Effective capacity [mAh]	Actual SOH [%]	Sublot
APR-EH171000702406	1100	1053.0	95.72	1
APR-EH171000707606		1049.6	95.41	1
APR-EH171000705424		1009.6	91.78	2
APR-EH171000711443		1015.4	92.30	2
APR-EH171000814013		976.4	88.76	3
APR-EH171000708804		971.9	88.35	3
APR-EH171000707901		966.0	87.81	3
APR-EH171000714657		947.32	86.12	4
APR-EH171000711199		945.01	85.91	4
APR-EH171000701957		944.46	85.86	4

Each testing phase involves checking two batteries with different SOH and SOC values. The SOC values were chosen based on the storing conditions by deposits or clients as follows: charged according to the standard storage procedure, with SOC considered at 40%; partially charged after long-term storage, with SOC considered at 80%; and fully charged with SOC considered as 95%-100%. Therefore, the following operating scenarios will be considered for system validation:

- Scenario 1: Battery 1 SOH 86% - SOC 80%, Battery 2 SOH 88% - SOC 80%, FW Buck operating mode.
- Scenario 2: Battery 1 SOH 86% - SOC 95%, Battery 2 SOH 95% - SOC 40%, RE Buck operating mode.
- Scenario 3: Battery 1 SOH 88% - SOC 95%, Battery 2 SOH 92% - SOC 40%, RE Buck operating mode.
- Scenario 4: Battery 1 SOH 86% - SOC 80%, Battery 2 SOH 92% - SOC 40%, FW Buck operating mode.
- Scenario 5: Battery 1 SOH 88% - SOC 80%, Battery 2 SOH 95% - SOC 40%, FW Buck operating mode.

Two data sets (Tables 2 and 3) were performed to ensure the results were redundant. The data obtained for verification (Table 3) will also be used to validate the sorting method.

Table 2

Experimental data obtained following the application of the algorithm for determining the internal resistance of batteries

Scenario	1	2	3	4	5
ID1	LFP11_001_78_085	LFP11_003_94_083	LFP11_005_92_072	LFP11_007_81_080	LFP11_009_77_077
ID2	LFP11_002_80_075	LFP11_004_41_045	LFP11_006_37_056	LFP11_008_40_058	LFP11_010_39_048
Technology	LFP				
Capacity [Ah]	1.1				
Ipulse [A]	±0.375				
OCV1 [V]	3.319	3.340	3.338	3.323	3.318
OCV2 [V]	3.322	3.267	3.259	3.265	3.263
SOC1 [%]	78.07	94.29	92.77	81.17	77.29
SOC2 [%]	80.40	41.96	37.62	40.84	39.74
Vdt1 [V]	0.032	0.031	0.027	0.030	0.029
Vdt2 [V]	0.029	0.017	0.021	0.022	0.018
Rin1 [Ω]	85.79	83.11	72.39	80.43	77.75
Rin2 [Ω]	75.07	45.45	56.15	58.82	48

Table 3

Second experimental data obtained following the application of the algorithm for determining the internal resistance of batteries

Scenario	1	2	3	4	5
ID1	LFP11_011_78_082	LFP11_013_94_085	LFP11_015_92_072	LFP11_017_78_080	LFP11_019_78_074
ID2	LFP11_012_79_077	LFP11_014_42_048	LFP11_016_38_058	LFP11_018_43_056	LFP11_020_40_045
Tehnology	LFP				
Capacity [Ah]	1.1				
Ipulse [A]	±0.375				
OCV1 [V]	3.319	3.34	3.338	3.319	3.319
OCV2 [V]	3.321	3.268	3.26	3.27	3.265
SOC1 [%]	78.07	94.29	92.77	78.07	78.07
SOC2 [%]	79.62	42.53	38.14	43.69	40.84
Vdt1 [V]	0.031	0.032	0.027	0.030	0.028
Vdt2 [V]	0.027	0.018	0.022	0.021	0.017
Rin1 [Ω]	82.67	85.56	72	80.43	74.67
Rin2 [Ω]	77.33	48.13	58.98	56.15	45.33

Table 4

The groups of batteries after the sorting procedure

	Battery ID	Corresponding battery	Internal resistance [mΩ]
Group 1	LFP11_001_84_085	EH171000714657	85.79
	LFP11_013_94_085	EH171000701957	85.56
Group 2	LFP11_007_81_080	EH171000711199	80.43
	LFP11_009_77_077	EH171000814013	77.75
	LFP11_003_95_083	EH171000701957	83.11
	LFP11_011_78_082	EH171000714657	82.67
	LFP11_012_79_077	EH171000707901	77.33
	LFP11_017_78_080	EH171000711199	80.43
Group 3	LFP11_004_40_045	EH171000702406	45.45
	LFP11_010_39_048	EH171000707606	48
	LFP11_014_42_048	EH171000702406	48.13
	LFP11_020_40_045	EH171000707606	45.33
Group 4	LFP11_006_37_056	EH171000705424	56.15
	LFP11_008_40_058	EH171000711443	58.82
	LFP11_016_38_058	EH171000705424	58.98
	LFP11_018_43_056	EH171000711443	56.15
Group 5	LFP11_005_92_072	EH171000708804	72.39
	LFP11_015_92_072	EH171000708804	72
	LFP11_002_80_075	EH171000707901	75.07
	LFP11_019_78_074	EH171000814013	74.67

Table 5

Results obtained after applying the grouping method

	Group 1	Group 2	Group 3	Group 4	Group 5
Average [mΩ]	85.67	80.28	46.72	57.52	73.53
Standard deviation [mΩ]	0.16	2.40	1.54	1.58	1.56
Range of values [mΩ]	85.51-85.83	77.88-82.68	45.18-48.27	55.93-59.11	71.97-75.09
Accepted batteries	LFP11_001_84_085 LFP11_013_94_085	LFP11_007_81_080 LFP11_003_95_083 LFP11_011_78_082 LFP11_017_78_080	LFP11_004_40_045 LFP11_010_39_048 LFP11_014_42_048 LFP11_020_40_045	LFP11_006_37_056 LFP11_008_40_058 LFP11_016_38_058 LFP11_018_43_056	LFP11_005_92_072 LFP11_015_92_072 LFP11_002_80_075 LFP11_019_78_074
SOH [%]	86	86-88	95	92	88
Battery closest to average	LFP11_001_84_085 LFP11_013_94_085	LFP11_007_81_080 LFP11_017_78_080	LFP11_014_42_048	LFP11_006_37_056 LFP11_018_43_056	LFP11_005_92_072

Therefore, groups of batteries were formed in 10 mΩ increments, starting with the battery with the lowest internal resistance (Table 4).

Next, the mean value and standard deviation were calculated for each group, and it was checked whether there were any gross errors in the range of ±σ. Also, it was determined which battery had the internal resistance closest to the mean value so that only one battery could be subjected to the SOH evaluation process. The results are presented in Table 5.

The dependency between SOC and OCV is independent of SOH, and the dependency between SOH and Rin is independent of SOC, so one of the variables must be known. Thus, SOC and Rin are determined according to the previously presented procedure, and based on the SOC, the internal resistance at the current SOC and at 100% SOC is estimated. The difference between the two is then added to the measured internal resistance. The new internal resistance, corresponding to 100% SOC and the current SOH, is compared to the internal resistance at 100% SOC and SOH. Suppose the internal resistance is greater than that at 100% SOH after the comparison. The method is validated in that case, confirming that the studied battery has a different SOH than a new one. For modelling the dependency between internal resistance and SOC, linear regression with a third-order polynomial was used to approximate the trend during both charging and discharging, as shown in Fig. 6.

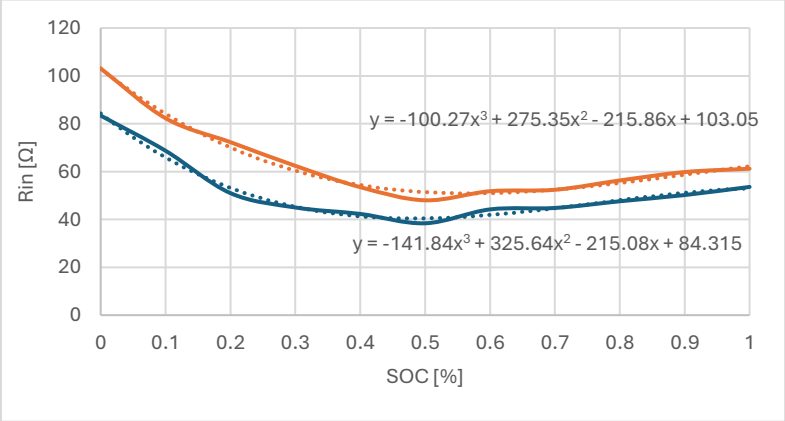

Fig. 6. The internal resistance estimation model, Rchg (blue) and Rdchg (Orange).

The characteristic equations for the internal resistance model for charge and discharge, respectively, are presented in equations (2) and (3):

$$R_{dchg} = -100.27 \cdot SOC^3 + 275.35 \cdot SOC^2 - 215.86 \cdot SOC + 103.05 \quad (2)$$

$$R_{chg} = -141.84 \cdot SOC^3 + 325.64 \cdot SOC^2 - 215.08 \cdot SOC + 84.315 \quad (3)$$

By applying the two equations for the first group of batteries LFP11_001_84_085 and LFP11_013_94_085, we obtain the following:

$$R_{dchg} = -100.27 \cdot 0.94^3 + 275.35 \cdot 0.94^2 - 215.86 \cdot 0.94 + 103.05 = 60.15\ m\Omega \quad (4)$$

$$R_{chg} = -141.84 \cdot 0.84^3 + 325.64 \cdot 0.84^2 - 215.08 \cdot 0.84 + 84.315 = 49.35\ m\Omega \quad (5)$$

For 100% SOC the internal resistances will be:

$$R_{dchg100} = -100.27 \cdot 1^3 + 275.35 \cdot 0.1^2 - 215.86 \cdot 1 + 103.05 = 62.27\ m\Omega \quad (6)$$

$$R_{chg100} = -141.84 \cdot 1^3 + 325.64 \cdot 1^2 - 215.08 \cdot 1 + 84.315 = 53.03\ m\Omega \quad (7)$$

The difference between resistance becomes:

$$\Delta R_{dchg} = 62.27\ m\Omega - 60.15\ m\Omega = 2.11\ m\Omega \quad (8)$$

$$\Delta R_{chg} = 53.03\ m\Omega - 49.35\ m\Omega = 3.68\ m\Omega \quad (9)$$

Next, this difference is added to the measured values and compared with the estimated values at 100% SOC and SOH:

$$R_{LFP11-001-84-085} = 2.11\ m\Omega + 85.79\ m\Omega = 87.90\ m\Omega \Rightarrow 87.90\ m\Omega > 62.27\ m\Omega \quad (10)$$

$$R_{LFP11-013-94-085} = 3.68\ m\Omega + 85.56\ m\Omega = 89.24\ m\Omega \Rightarrow 89.24\ m\Omega > 53.03\ m\Omega \quad (11)$$

The batteries' internal resistance is higher than the estimated internal resistance of a fresh cell at 100% SOC and SOH. Moreover, the results seem to be the same regardless of the pulse type, charge, or discharge. Table 6 presents the internal resistance values of the other batteries and compares them with a fresh cell.

Table 6

Internal resistance at 100% SOC and SOH

Battery ID	Rin at 100% SOC & SOH [mΩ]	Higher than fresh cell?
$R_{LFP11-001-84-085}$	87.90	Yes
$R_{LFP11-013-94-085}$	89.24	Yes
$R_{LFP11-007-81-080}$	85.09	Yes
$R_{LFP11-003-95-083}$	84.86	Yes
$R_{LFP11-011-78-082}$	88.34	Yes
$R_{LFP11-017-78-080}$	88.08	Yes
$R_{LFP11-004-40-045}$	57.17	Yes

$R_{LFP11-010-39-048}$	59.48	Yes
$R_{LFP11-014-42-048}$	60.24	Yes
$R_{LFP11-020-40-045}$	57.05	Yes
$R_{LFP11-006-36-056}$	67.05	Yes
$R_{LFP11-008-40-058}$	70.54	Yes
$R_{LFP11-016-38-058}$	65.96	Yes
$R_{LFP11-018-43-056}$	65.24	Yes
$R_{LFP11-005-92-072}$	75.22	Yes
$R_{LFP11-015-92-072}$	74.83	Yes
$R_{LFP11-002-80-075}$	80.06	Yes
$R_{LFP11-019-78-074}$	80.34	Yes

After the sorting process was applied, five groups were determined, followed by the grouping method where two batteries were eliminated from group 2. Then, for each battery, the actual internal resistance at 100% SOC was calculated and compared with that of a fresh cell at 100% SOC and SOH. The results indicate the correct identification of the battery groups, although batteries with SOH of 86% and 88% were mixed in three groups. However, these results fall within the error suggested in the literature and the USABC manual of 2%. Once the batteries are sorted, they are ready to be grouped and integrated into a battery module, which can be utilized in low-power applications based on the newly determined effective capacity. However, these second-life applications come with certain restrictions due to safety limitations. In this new configuration, the battery module will be exposed to a 15-20% lower discharge current, ranging from 0.5C to 0.8C of the new effective capacity. Additionally, thermal restrictions will be adjusted with the same coefficients to prevent fire hazards. All these modifications will be reflected in the new Battery Management System (BMS) that will equip the second-life battery.

5. Conclusions

To validate the proposed system, experiments were conducted using ten LFP battery cells grouped into four sub-lots based on their SOH. Each sub-lot represented different ageing levels, ranging from 86% to 95% SOH. The cascaded Buck-Boost DC-DC converter played a central role in the testing process, facilitating simultaneous charge-discharge testing. The control and monitoring of the system were managed by an ESP32 microcontroller, which ensured precise regulation of the testing parameters and implemented safety protocols to prevent overcharging and overheating. The findings confirmed that the internal resistance-based presorting stage effectively identified groups of batteries with homogeneous characteristics within a 2% SOH error margin.

The rapid multi-chemistry and multi-battery screening system for retired Lithium-Ion batteries proposed in this study offers a transformative approach to battery evaluation, classification, and repurposing from the point of view of testing time, costs, and adaptability. In this study, a new methodology is proposed, based on internal resistance measurement, by integrating a presorting stage before the actual screening. The rapid grouping of batteries with similar internal resistance minimizes the need for comprehensive SOH evaluations on every individual battery, and accuracy is achieved by subjecting only one representative battery from the group to the slow screening method. Moreover, the modular design of the sorting system, centered around the cascaded Buck-Boost DC-DC converter, allows for simultaneous testing of two or more batteries, which reduces the testing time by half. Because of the high-power density and the converter's wide input/output voltage range, the solution can be easily adapted to complex battery configurations and battery chemistry.

Acknowledgement

This work was supported by a grant of the Ministry of Research, Innovation and Digitalization, project number PNRR-C9-I8-760090/23.05.2023, code CF 30/14.11.2022.

REFERENCES

[1] T. Wu, S. Liu, Z. Wang, and Y. Huang, "SOC and SOH Joint Estimation of Lithium-Ion Battery Based on Improved Particle Filter Algorithm," J. Electr. Eng. Technol., vol. 17, no. 1, pp. 307–317, Jan. 2022, doi: 10.1007/s42835-021-00861-y.

[2] P. Mei et al., "Battery state estimation methods and management system under vehicle–cloud collaboration: A Survey," Renew. Sustain. Energy Rev., vol. 206, p. 114857, Dec. 2024, doi: 10.1016/j.rser.2024.114857.

[3] I. Stefan and K. Chirumalla, "Enabling value retention in circular ecosystems for the second life of electric vehicle batteries," Resour. Conserv. Recycl., vol. 212, p. 107942, Jan. 2025, doi: 10.1016/j.resconrec.2024.107942.

[4] K. Neigum and Z. Wang, "Technology, economic, and environmental analysis of second-life batteries as stationary energy storage: A review," J. Energy Storage, vol. 103, p. 114393, Dec. 2024, doi: 10.1016/j.est.2024.114393.

[5] J. Zhang, P. Wang, Q. Gong, and Z. Cheng, "SOH estimation of lithium-ion batteries based on least squares support vector machine error compensation model," J. Power Electron., vol. 21, no. 11, pp. 1712–1723, Nov. 2021, doi: 10.1007/s43236-021-00307-8.

[6] C. Zhang, J. Marco, and T. Fai Yu, "Hardware Platform Design of Small Energy Storage System Using Second Life Batteries," in 2018 UKACC 12th International Conference on Control (CONTROL), Sheffield: IEEE, Sep. 2018, pp. 163–168. doi: 10.1109/CONTROL.2018.8516871.

[7] Z. Kolková, J. Jandík, J. Novotný, A. Zubo, and J. Matušov, "Topology and Main System Components in Second-Life Battery Energy Storage Systems," in 2024 ELEKTRO

(ELEKTRO), Zakopane, Poland: IEEE, May 2024, pp. 1–4. doi: 10.1109/ELEKTRO60337.2024.10556974.

[8] E. Hossain, D. Murtaugh, J. Mody, H. M. R. Faruque, Md. S. Haque Sunny, and N. Mohammad, "A Comprehensive Review on Second-Life Batteries: Current State, Manufacturing Considerations, Applications, Impacts, Barriers & Potential Solutions, Business Strategies, and Policies," IEEE Access, vol. 7, pp. 73215–73252, 2019, doi: 10.1109/ACCESS.2019.2917859.

[9] J. Zhu et al., "End-of-life or second-life options for retired electric vehicle batteries," Cell Rep. Phys. Sci., vol. 2, no. 8, p. 100537, Aug. 2021, doi: 10.1016/j.xcrp.2021.100537.

[10] S. Yang, C. Zhang, J. Jiang, W. Zhang, L. Zhang, and Y. Wang, "Review on state-of-health of lithium-ion batteries: Characterizations, estimations and applications," J. Clean. Prod., vol. 314, p. 128015, Sep. 2021, doi: 10.1016/j.jclepro.2021.128015.

[11] G. Piłatowicz, A. Marongiu, J. Drillkens, P. Sinhuber, and D. U. Sauer, "A critical overview of definitions and determination techniques of the internal resistance using lithium-ion, lead-acid, nickel metal-hydride batteries and electrochemical double-layer capacitors as examples," J. Power Sources, vol. 296, pp. 365–376, Nov. 2015, doi: 10.1016/j.jpowsour.2015.07.073.

[12] E. Braco, I. San Martín, P. Sanchis, and A. Ursúa, "Fast capacity and internal resistance estimation method for second-life batteries from electric vehicles," Appl. Energy, vol. 329, p. 120235, Jan. 2023, doi: 10.1016/j.apenergy.2022.120235.

[13] H. Tian, P. Qin, K. Li, and Z. Zhao, "A review of the state of health for lithium-ion batteries: Research status and suggestions," J. Clean. Prod., vol. 261, p. 120813, Jul. 2020, doi: 10.1016/j.jclepro.2020.120813.

[14] Q.-Q. Liu, B. Chen, and J. Zhang, "Life prediction of satellite lithium battery based on multi time-scale extended Kalman Filter (EKF) Algorithm".

[15] N.-T. Pham, P.-H. La, and S.-J. Choi, "Online cell-by-cell SOC/SOH estimation method for battery module employing extended Kalman filter algorithm with aging effect consideration," J. Power Electron., vol. 22, no. 12, pp. 2092–2099, Dec. 2022, doi: 10.1007/s43236-022-00526-7.

[16] L. Cong, W. Wang, and Y. Wang, "A review on health estimation techniques of end-of-first-use lithium-ion batteries for supporting circular battery production," J. Energy Storage, vol. 94, p. 112406, Jul. 2024, doi: 10.1016/j.est.2024.112406.

[17] R. Guo and W. Shen, "Recent advancements in battery state of power estimation technology: A comprehensive overview and error source analysis," J. Energy Storage, vol. 103, p. 114294, Dec. 2024, doi: 10.1016/j.est.2024.114294.

[18] A. Berrueta, I. S. Martin, J. Pascual, P. Sanchis, and A. Ursua, "On the requirements of the power converter for second-life lithium-ion batteries," in 2019 21st European Conference on Power Electronics and Applications (EPE '19 ECCE Europe), Genova, Italy: IEEE, Sep. 2019, p. P.1-P.8. doi: 10.23919/EPE.2019.8915006.

[19] L. Wen-Di et al., "Design of battery management system for energy storage equipment of the tethered aerostat".

[20] T.-I. Voicila, G.-C. Seritan, B.-A. Enache, M. Stanculescu, and R.-F. Porumb, "Design and implementation of a multi-battery, multi-chemistry state of health screening system," in 2023 10th International Conference on Modern Power Systems (MPS), Cluj-Napoca, Romania: IEEE, Jun. 2023, pp. 1–4. doi: 10.1109/MPS58874.2023.10187442.

[21] G. Hunt, “USABC electric vehicle battery test procedures manual.” USA: United States Department of Energy, 1996.

[22] T.-I. Voicilă, G.-C. Seriţan, B.-A. Enache, R. Porumb, and M. Stănculescu, “First Steps Towards the Design of a multi-Chemistry, multi-Battery State of Health Screening System,” in 2023 13th International Symposium on Advanced Topics in Electrical Engineering (ATEE), Bucharest, Romania: IEEE, Mar. 2023, pp. 1–6. doi: 10.1109/ATEE58038.2023.10108169.